Electronic Supplementary Material (ESI) for Nanoscale Horizons.

Supporting Information

Subnanometer Iron Clusters Confined in Porous Carbon Matrix for Highly Efficient Zinc–Air Batteries

Xin Wu, Juncai Dong, Mei Qiu, Yang Li, Yongfan Zhang, Huabin Zhang,* and Jian Zhang*

Experimental Section

Synthesis of PCN-222: PCN-222 was synthesized by a solvothermal reaction. A mixture of 50 mg $ZrCl_4$, 50 mg tetrakis (4-carboxyphenyl) porphyrin (TCPP) and 2.7 g benzoic acid in N, N-diethylformamide (DEF) was heated for two days at 120 ^{o}C. PCN-222 was obtained after thoroughly washing with water and ethanol, then drying at 60 ^{o}C under vacuum.[S1-S2]

Synthesis of Fe-Fe@NC and Fe@NC: Ferric nitrate (20 mg) was dissolved into N, N-dimethylformamide (DMF, 10 mL). PCN-222 (100 mg) was transformed to the solution, then heated at 120 ^{o}C for one day. After thoroughly washing with water and ethanol, then drying at 60 ^{o}C under vacuum, the obtained PCN-222(Fe) was pyrolyzed at 800 ^{o}C for 2 h with a heating rate of 5 ^{o}C/min under nitrogen atmosphere. The pyrolyzed networks were subjected to acid (HF, 5 wt % in water) washing for one day, then washing with water and ethanol and drying at 60 ^{o}C under vacuum. The loading amount of Fe is confirmed to be 0.93 wt% by inductively coupled plasma optical emission spectrometry (ICP-OES). Fe@NC was obtained by a similar method except that the amount of added ferric nitrate was reduced to 10 mg.

Synthesis of Fe-NP/C: Ferric nitrate (50 mg) and meso-tetraphenylporphyrin (TPP, 100 mg) were dissolved into 100 mL DMF. The mixture was reacted at 120 ^{o}C for one day. After cooling down to room temperature, TPP(Fe) was obtained after removing DMF. After washing with water and ethanol, then dried under vacuum at 60 ^{o}C, the obtained TPP(Fe) was pyrolyzed at 800 ^{o}C for 2 h with a heating rate of 5

^{o}C/min under a N_2 atmosphere to finally get the product Fe-NP/C. The loading amount of Fe is confirmed to be 0.51 wt% by ICP-OES.

Synthesis of NC: The obtained PCN-222 was pyrolyzed at 800 ^{o}C for 2 h with a heating rate of 5 ^{o}C/min under a N_2 atmosphere. The pyrolyzed networks were subjected to acid (HF, 5 wt % in water) washing for one day, and then washed with water and ethanol, dried under vacuum at 60 ^{o}C.

Materials characterization: X-ray diffraction (XRD) patterns were recorded from 10^o to 80^o by employing an X-ray diffractometer with Cu-Kα radiation at 30 kV and 20 mA. The step degree is 0.02^o/s and the scanning speed is 5^o/min. The morphology was determined by scanning electron microscope (SEM) combined with transmission electron microscope (TEM), using a JEOL JSM6700-F microscope and FEI Tecnai F20, respectively. In addition, the high-angle annular dark-field scanning transmission electron microscopy (HAADF-STEM) image was obtained using a spherical aberration-corrected STEM (JEOL JEM-ARF200F). A Micromeritics ASAP 2020 System was used to investigate surface area. Surface composition and oxidation states were investigated through a Thermo Scientific ESCALAB 250Xi X-ray photoelectron spectroscopy (XPS) system. The Fe K-edge extended X-ray absorption fine structure (EXAFS) spectra were acquired at the beamline 1W1B of the Beijing Synchrotron Radiation Facility in a fluorescence mode. The EXAFS raw data were processed with the IFEFFIT package.[S3-S4]

Electrochemical measurements: To prepare the working electrodes, 5 mg catalysts and Nafion solution (50 μL, 5 wt%) were dispersed in 450 μL ethanol for sonication to form a homogeneous ink. 3 μL ink was loaded onto the glassy carbon electrode of 0.196 cm^2 surface. The electrochemical measurements were carried out in a three-electrode cell using a glass carbon rotating disk electrode (5 mm in diameter, Pine) as working electrode. The reference electrode was Ag/AgCl, KCl (3 M). For the counter electrode, a Pt wire was used. CV analysis was performed at a scan rate of 10 mV s^{-1} in 0.1 M KOH. The linear sweep voltammetry (LSV) curves were obtained at 5 mV s^{-1}.

Fabrication of Zn-air battery: To test the activity of Fe-Fe@NC as catalyst in Zn-air batteries, a primary Zn-air battery was assembled with a zinc plate as the anode. The cathode was carbon cloth possessing two sides. The air-facing side is for gas diffusion with an effective area of 1 cm^2 and the water facing side is a catalyst layer. The catalyst layer was made by loading the catalyst ink prepared as described in electrocatalytic experiments onto the water-facing side with a loading of 2 mg cm^{-2}. 6.0 M KOH and 6 M KOH containing 0.2 M zinc acetate was employed as the electrolyte for the primary and rechargeable Zn-air batteries, respectively. Measurements were performed using a LAND testing system and electrochemical working station (Pine) at room temperature.

Computational methods: Calculations are performed based on DFT calculations using the VASP[S5] and PAW methods.[S6-S7] The N-doped grapheme was modeled with a 3x3 cell. The plane-wave cutoff energy was set to 400 eV and a 7 x 7 x 1 grid was used in the Monkhorst-Pack scheme. The conventional energy was 10^{-6} eV with a 0.02 eV/Å maximum force.

[S1]D. Feng, Z. Y. Gu, J. R. Li, H. L. Jiang, Z. Wei, H. C. Zhou, *Angew. Chem. Int. Ed.* 2012, **51**, 10307.

[S2]H. Q. Xu, J. Hu, D. Wang, Z. Li, Q. Zhang, Y. Luo, S. H. Yu, H. L. Jiang, *J. Am. Chem. Soc.* 2015, **137**, 13440.

[S3]B. Ravel, M. Newville, *J. Synchrotron Radiat.* 2005, **12**, 537.

[S4]D. C. Koningsberger, R. Eds. Prins, Wiley: *New York* 1988, **92**, 673.

[S5]G. Kresse, J. Hafner, *Phys. Rev. B* 1993, **47**, 558.

[S6]P. E. Blöchl, *Phys. Rev. B* 1994, **50**, 17953.

[S7]J. Hafner, *J. Comput. Chem*. 2008, **29**, 2044.

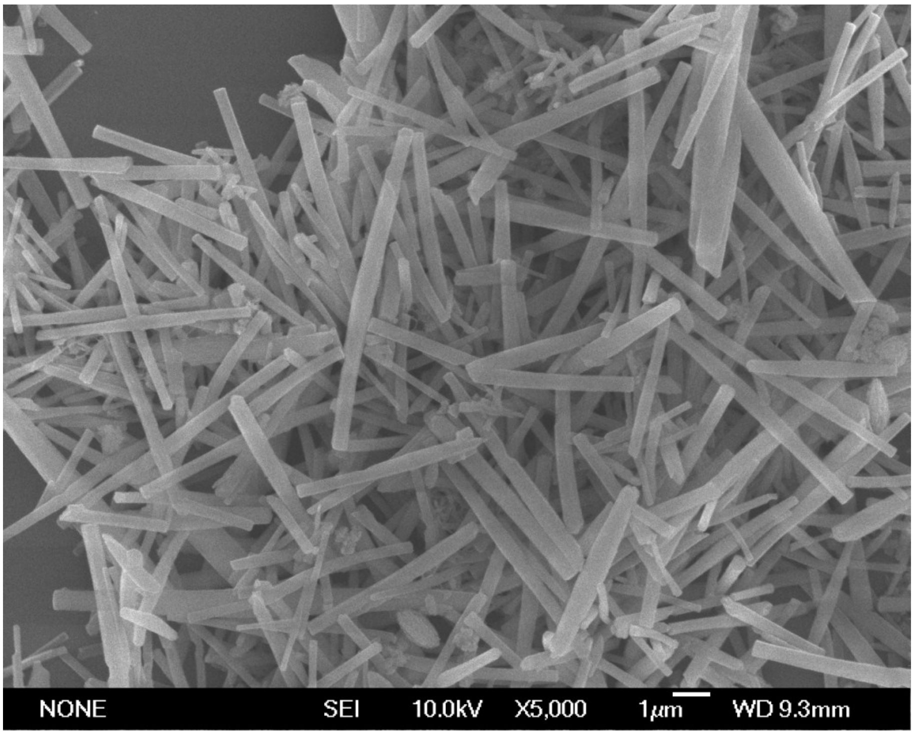

Fig. S1 The SEM image of PCN-222(Fe).

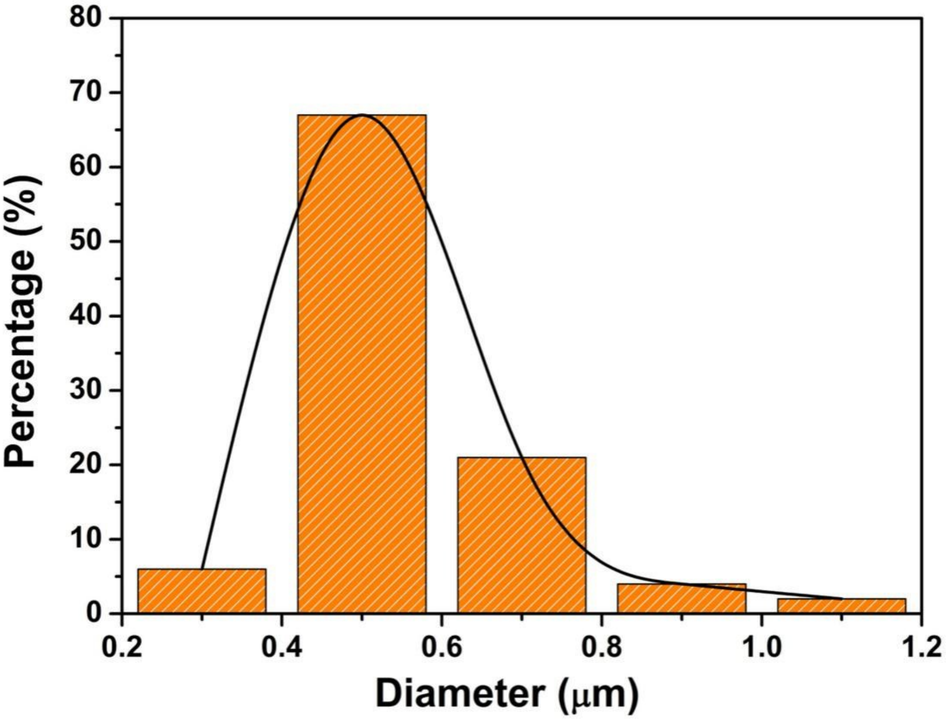

Fig. S2 Size distribution of PCN-222(Fe) evaluated from the SEM image of Figure S1. 100 crystals of PCN-222(Fe) were counted for analysis.

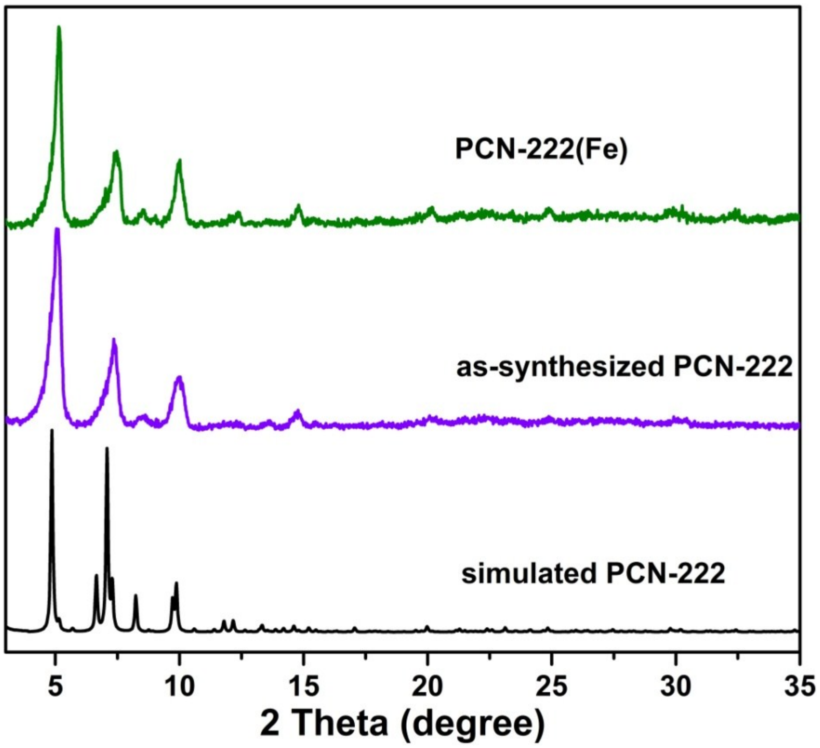

Fig. S3 The powder X-ray diffraction (PXRD) patterns of PCN-222 and PCN-222(Fe). The standard pattern PCN-222 has also been shown as a reference. After metalation of Fe, the PXRD patterns remained nearly unchanged, suggesting that the metalation doesn’t destroy the structure of PCN-222.

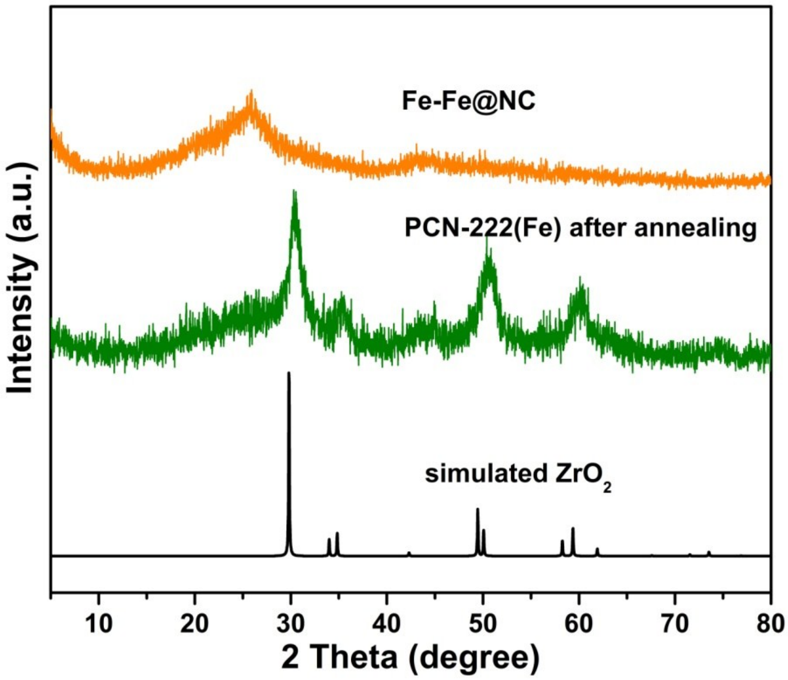

Fig. S4 The powder X-ray diffraction (PXRD) patterns of PCN-222(Fe) after annealing and Fe-Fe@NC. The standard pattern ZrO_2 has also been shown as a reference. ZrO_2 can be removed after leaching with dilute HF. There are no characteristic peaks of Fe in the samples, indicating low crystallinity and very small metal particles supported on carbon.

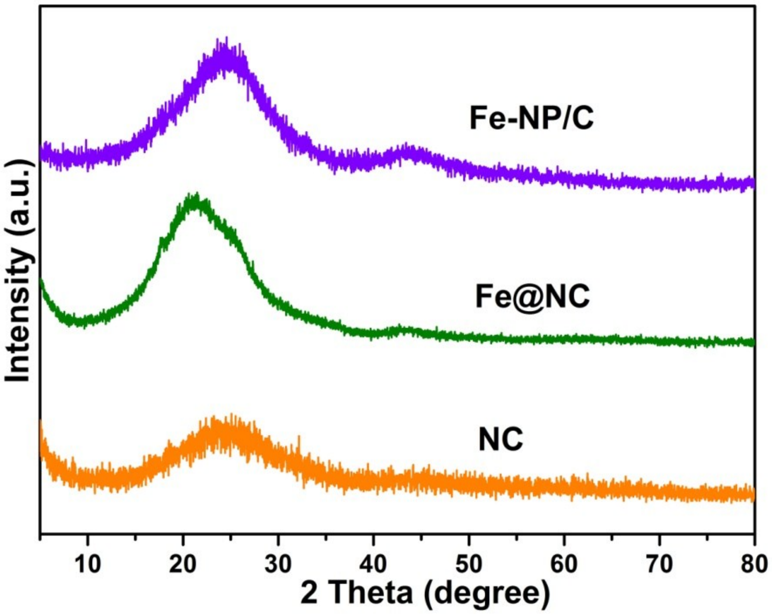

Fig. S5 The powder X-ray diffraction (PXRD) patterns of Fe-NP/C, Fe@NC and NC. There are no characteristic peaks of Fe in Fe-NP/C and Fe@NC, indicating low content and very small metal particles supported on carbon.

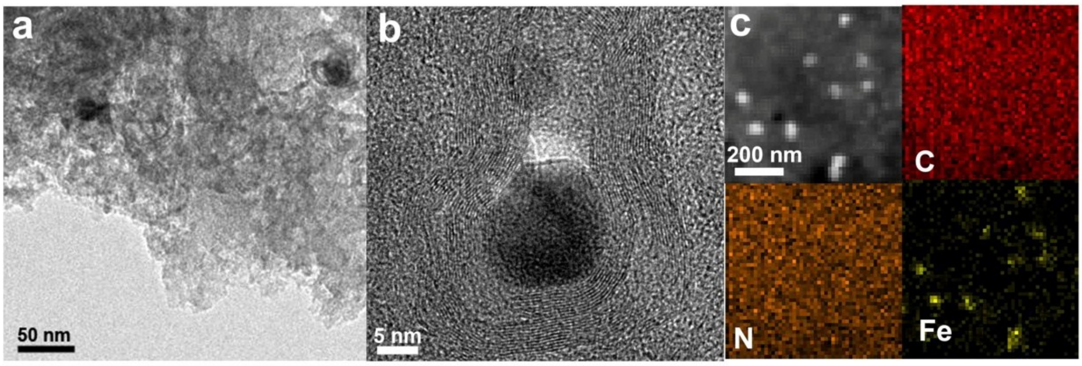

Fig. S6 (a,b) TEM images of Fe-NP/C. Small Fe-derived nanoparticles were clearly observed. (c) The STEM image of Fe-NP/C and the elemental distributions of C, N and Fe.

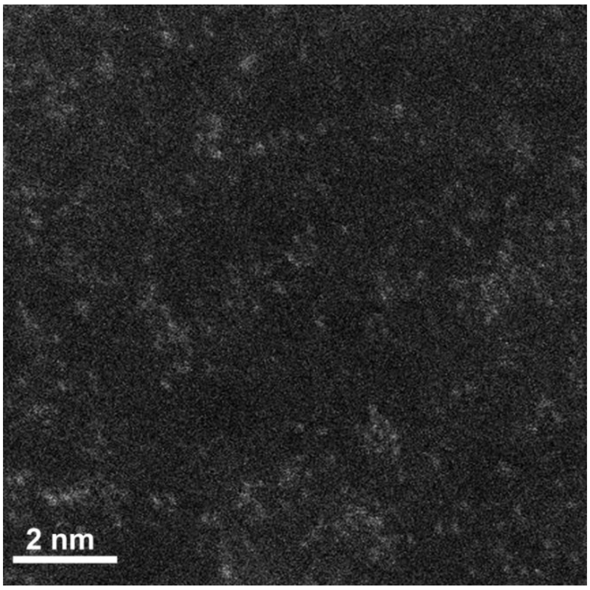

Fig. S7 The HAADF-STEM image of Fe@NC.

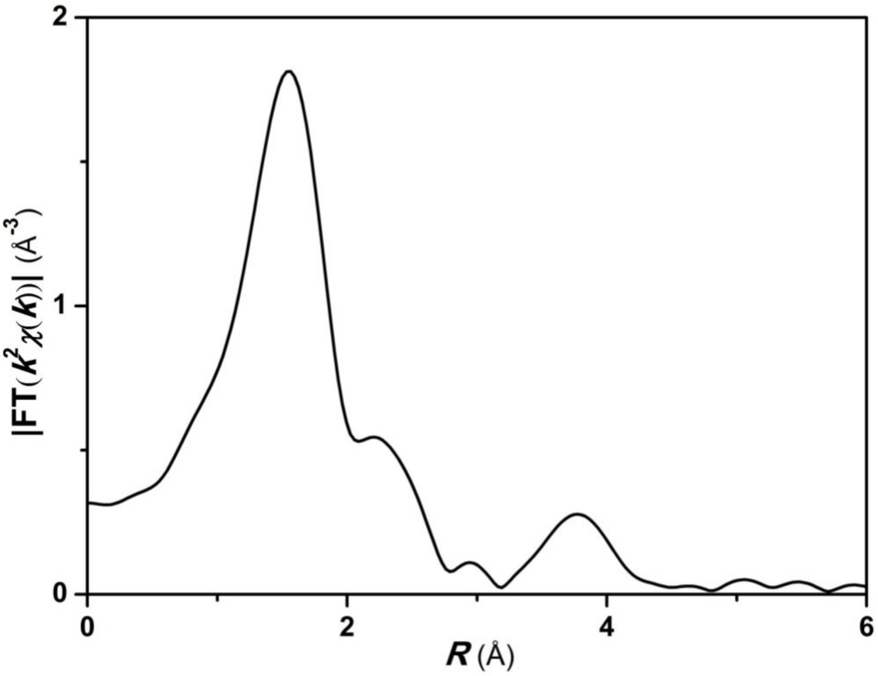

Fig. S8 Fe K-edge EXAFS spectrum of Fe@NC. It exhibits Fe-N interaction at 1.5 Å.

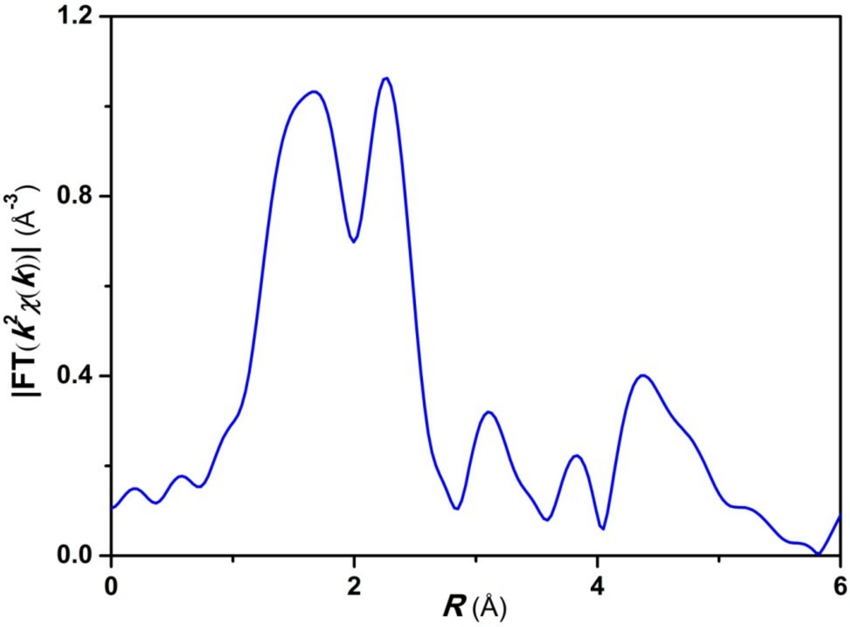

Fig. S9 Fe K-edge EXAFS spectrum of Fe-NP/C. It exhibits Fe-N/C interaction at 1.5 Å and Fe-Fe interaction at 2.2 Å.

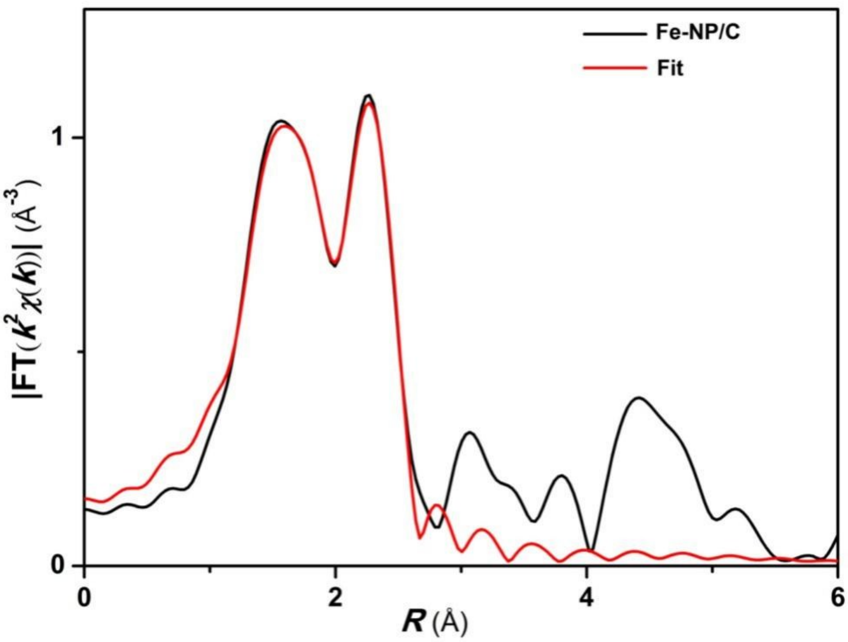

Fig. S10 Fourier transform of the experimental EXAFS spectrum in R space and the best fitting result for Fe-NP/C. Measured and calculated spectra are matched very well. The best-fit parameters are shown in Table S1.

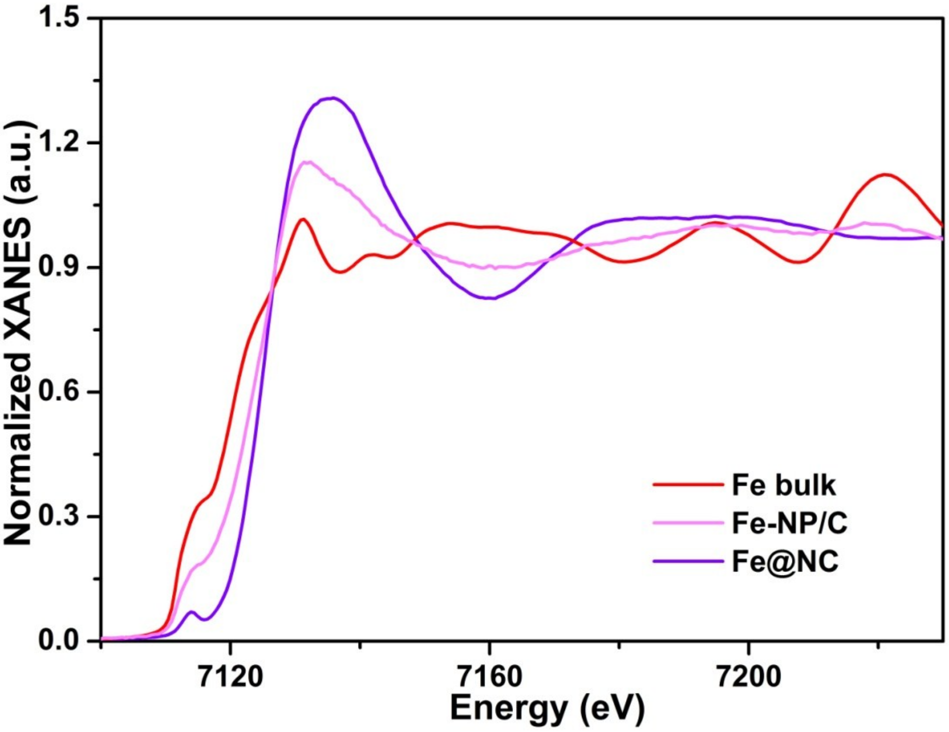

Fig. S11 The normalized Fe-edge XANES spectra of Fe@NC, Fe-NP/C and Fe bulk.

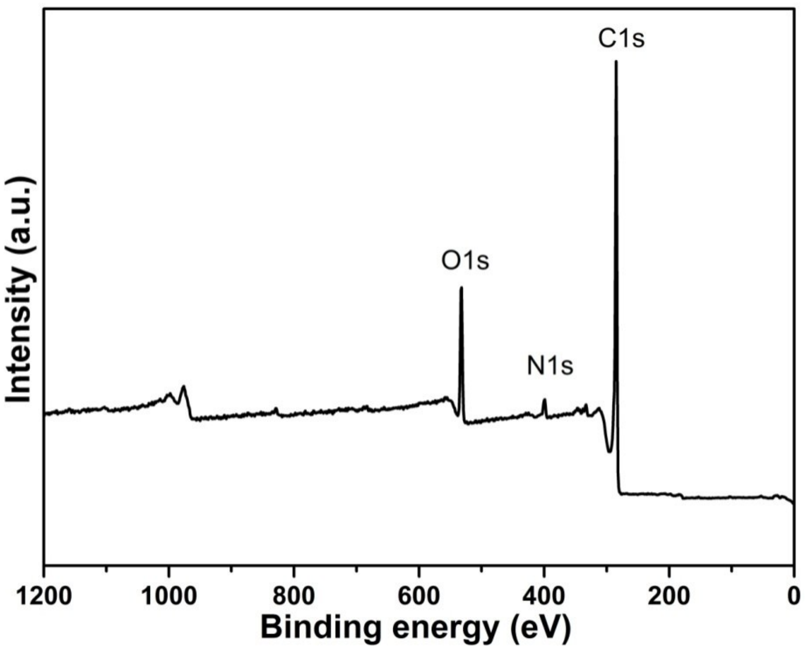

Fig. S12 Survey spectrum of XPS analysis of Fe-Fe@NC. No peaks of other elements except N, C and O are observed. The O peaks come mainly from the atmospheric contamination for the exposure to air. The absence of Fe signals may be attributed to the low amount of Fe subnanometer clusters determined by the ICP-OES.

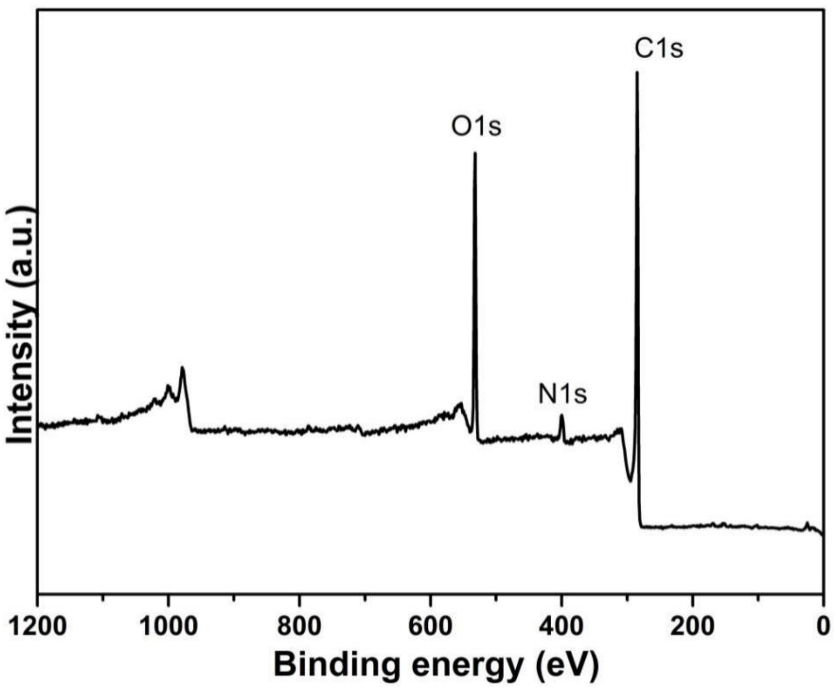

Fig. S13 Survey spectrum of XPS analysis of Fe-NP/C. No peaks of other elements except N, C and O are observed. The O peaks come mainly from the atmospheric contamination for the exposure to air. The absence of Fe signals may be attributed to the low amount of Fe nanoparticles determined by the ICP-OES.

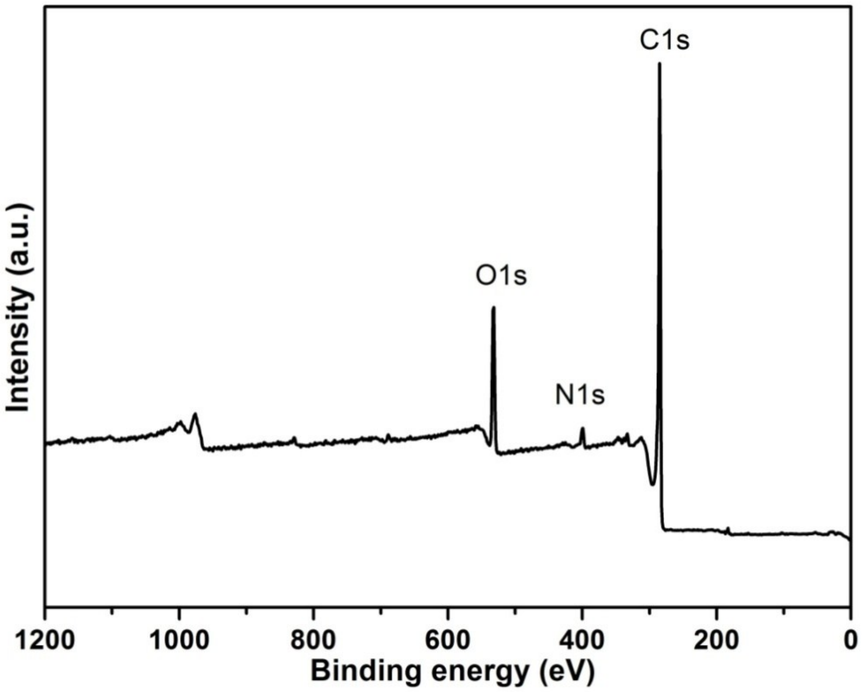

Fig. S14 Survey spectrum of XPS analysis of Fe@NC. No peaks of other elements except N, C and O are observed. The O peaks come mainly from the atmospheric contamination for the exposure to air. The absence of Fe signals may be attributed to the low amount of single Fe atoms determined by the ICP-OES.

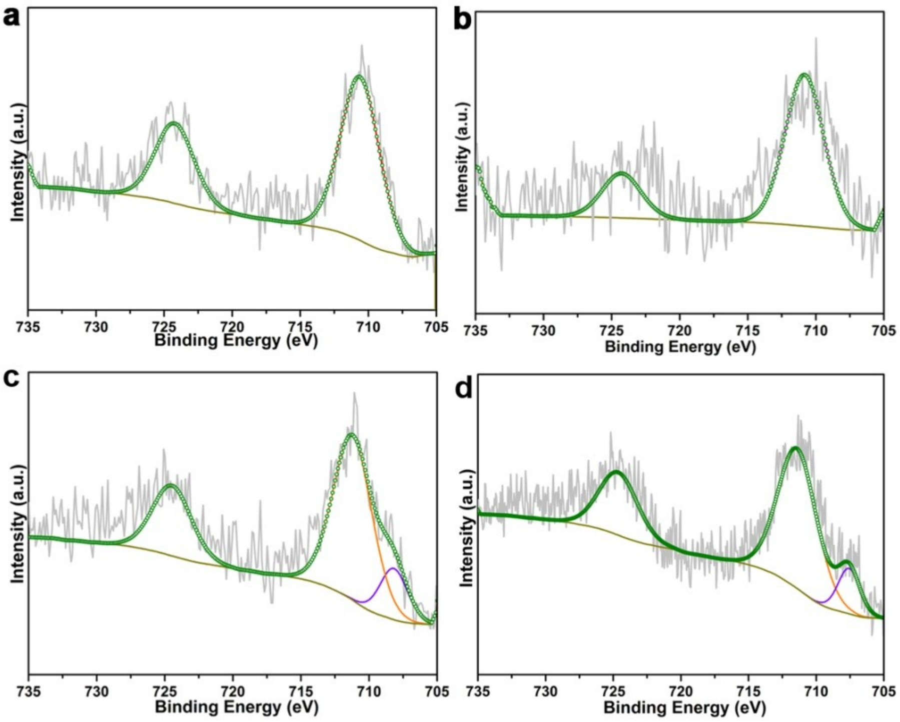

Fig. S15 (a) The XPS spectrum of Fe 2p for PCN-222(Fe), which shows two deconvoluted peaks for Fe^{2+} (724.4 and 711.3 eV). (b) The XPS spectrum of Fe 2p for Fe@NC, indicating the Fe-N interaction. (c) The XPS spectrum of Fe 2p for Fe-Fe@NC. (d) The XPS spectrum of Fe 2p for Fe-NP/C. The additional peak at ≈708 eV can be assigned to zero-valence metallic and the weak intensity is attributed to the small size of the aggregated metallic Fe.

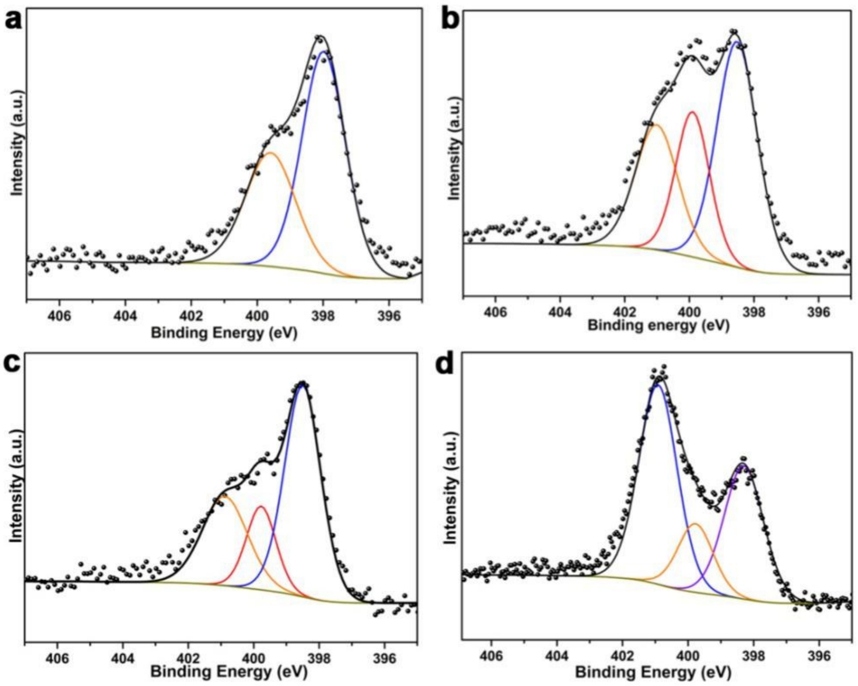

Fig. S16 The XPS spectrum of N 1s spectra for (a) PCN-222(Fe), (b) Fe@NC, (c) Fe-Fe@NC, (d) Fe-NP/C. The high-resolution spectra for nitrogen 1s of Fe@NC, Fe-Fe@NC and Fe-NP/C display three deconvoluted peaks corresponding to pyridinic nitrogen and/or Fe-N (398.5 eV), pyrrolic (399.5 eV) and graphitic nitrogen species (401.0 eV), respectively.

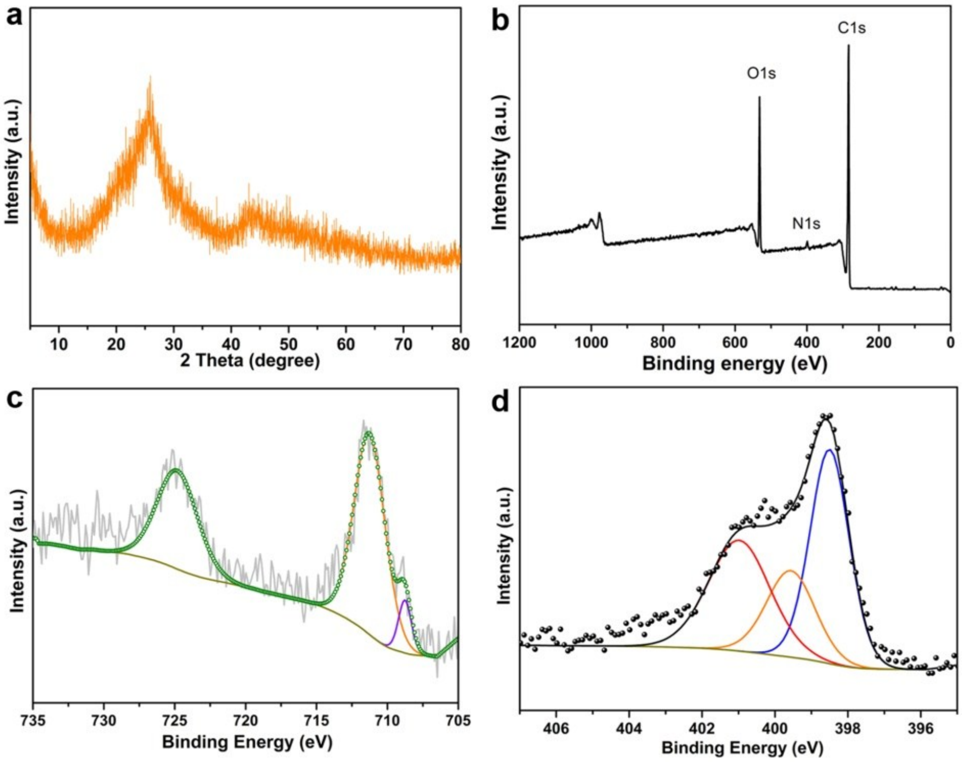

Fig. S17 (a) The powder X-ray diffraction (PXRD) patterns of Fe subclusters decorated catalyst with 15 mg ferric nitrate in the synthesized process. The corresponding XPS analysis of survey spectrum (b), Fe 2p spectrum (c) and N 1s spectrum (d). The peaks at 724.4 eV and 711.3 eV are ascribed to Fe-N interaction, the additional peak at ≈708 eV can be assigned to zero-valence metallic and the weak intensity is attributed to the small size of the aggregated metallic Fe. N 1s spectrum displays three deconvoluted peaks corresponding to pyridinic nitrogen and/or Fe-N (398.5 eV), pyrrolic (399.5 eV) and graphitic nitrogen species (401.0 eV), respectively.

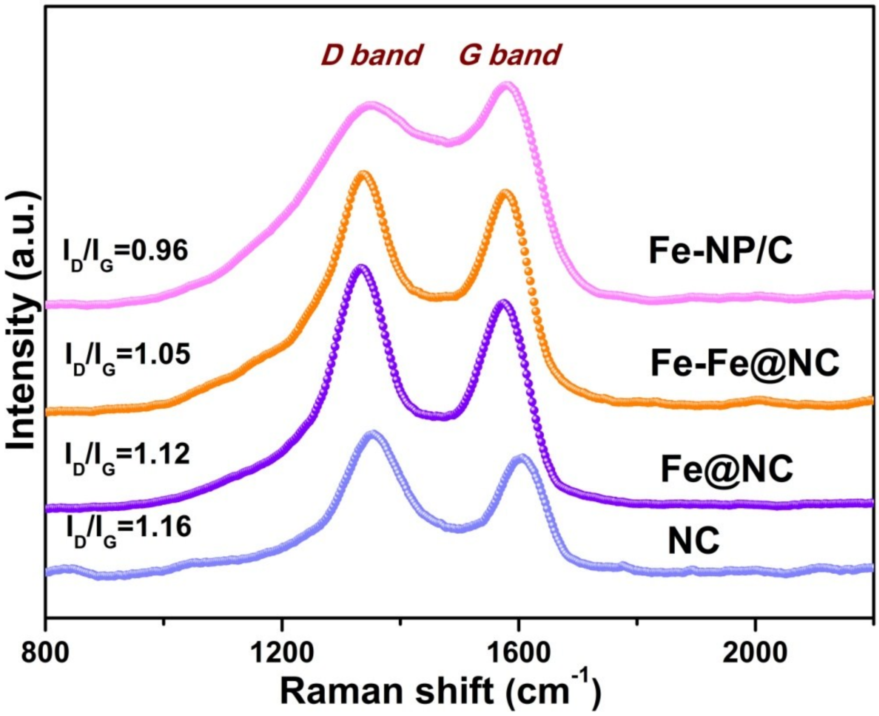

Fig. S18 Raman spectra of Fe-NP/C, Fe-Fe@NC, Fe@NC, and NC.

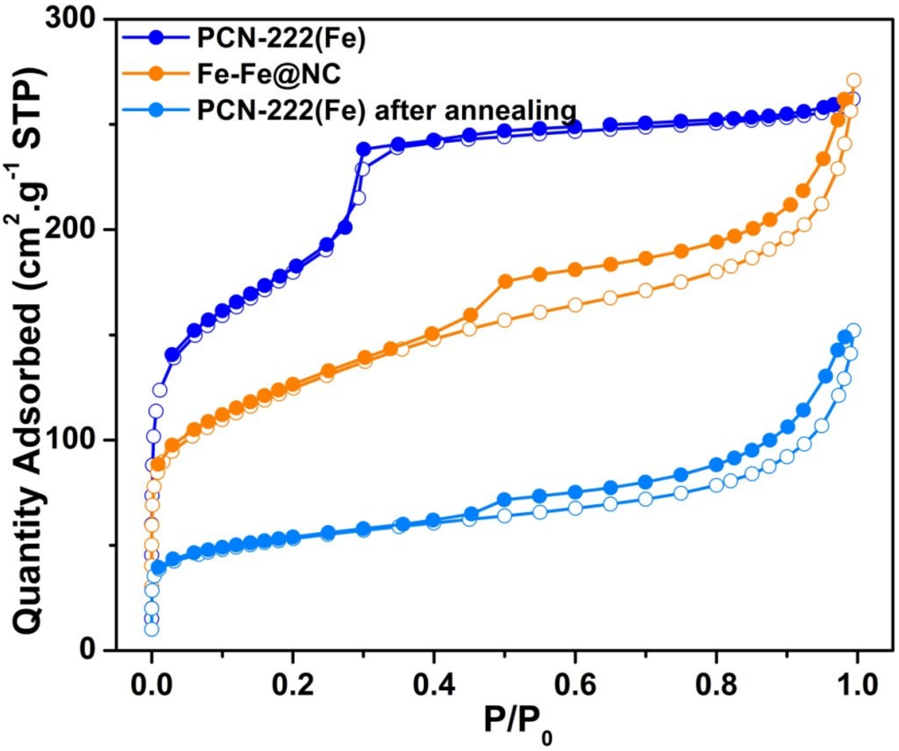

Fig. S19 The N_2 sorption isotherms examined at 77 K for PCN-222(Fe), Fe-Fe@NC and PCN-222(Fe) after annealing. The typical type IV isotherm of PCN-222(Fe) exhibits a steep increase at the point of P/P_0 = 0.3, suggesting microporosity. A N_2 uptake of 262 cm^3 g^{-1} (STP) and a Brunauer-Emmett-Teller (BET) surface area of 652 m^2 g^{-1} have been observed for PCN-222(Fe), without activation procedures. After pyrolysis, large hysteresis loops was observed in the sorption isotherms of N_2, indicating the presence of mesopores. It is worthwhile to notice that the absorbed volume observed for Fe-Fe@NC is remarkably larger than the direct pyrolysis product of PCN-222(Fe). A N_2 uptake of 152 cm^3 g^{-1} (STP) and a Brunauer-Emmett-Teller (BET) surface area of 180 m^2 g^{-1} have been observed for PCN-222(Fe) after annealing without leaching with dilute HF. A N_2 uptake of 270 cm^3 g^{-1} (STP) and a Brunauer-Emmett-Teller (BET) surface area of 433 m^2 g^{-1} have been observed for Fe-Fe@NC.

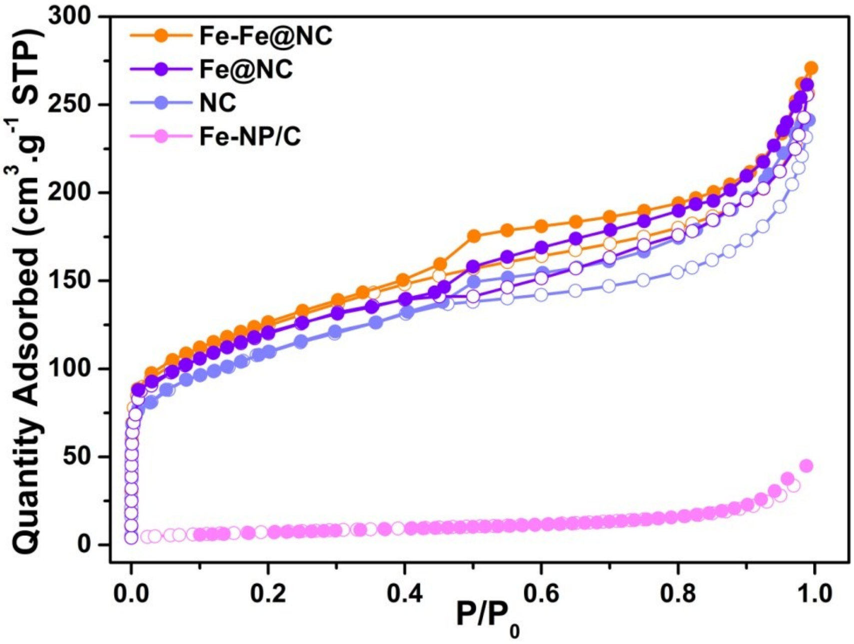

Fig. S20 The N_2 sorption isotherms examined at 77 K for Fe-Fe@NC, Fe@NC, NC and Fe-NP/C. Among them, Fe-Fe@NC, Fe@NC and NC retain the hierarchical porosity of the parent MOF while Fe-NP/C derived from complex exhibits a low N_2 uptake. Fe-Fe@NC maintains a highly accessible surface area, which may be ascribed to excessive carbon corrosion by Fe subcluster at such high pyrolysis temperature.

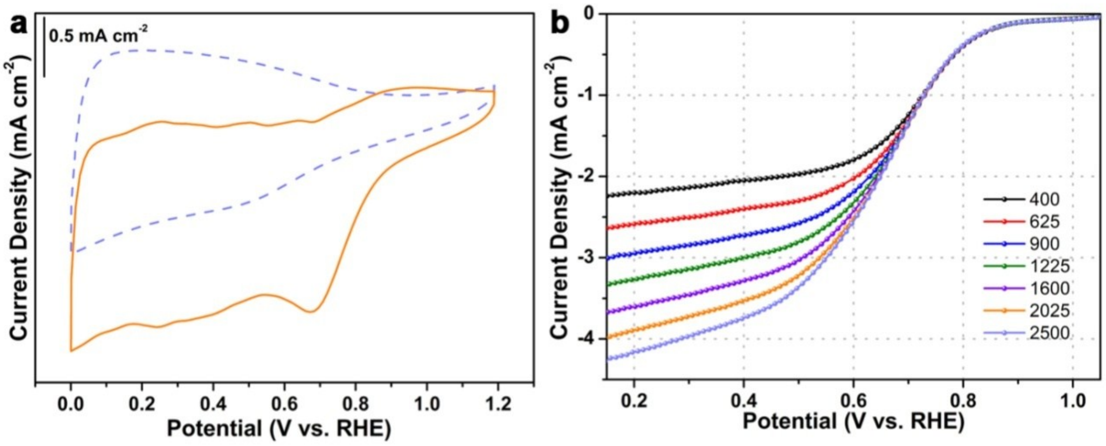

Fig. S21 (a) The CV curves of Fe@NC in O_2-saturated (solid line) or N_2-saturated (dash line) in 0.1 M KOH at a sweep rate of 10 mV s^{-1}; (b) The LSV curves of Fe@NC in O_2-saturated 0.1 M KOH at a sweep rate of 5 mV s^{-1}.

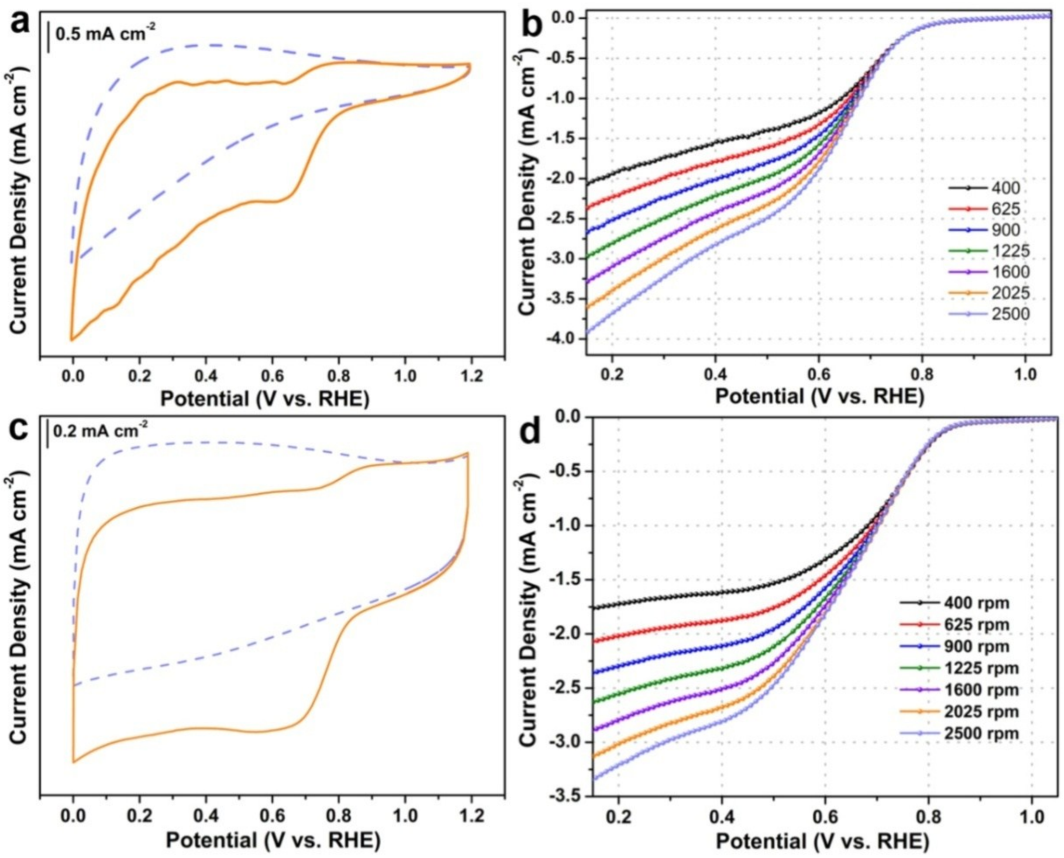

Fig. S22 (a) The CV curves of Fe-NP/C in O_2-saturated (solid line) or N_2-saturated (dash line) in 0.1 M KOH at a sweep rate of 10 mV s^{-1}; (b) The LSV curve of Fe-NP/C in O_2-saturated 0.1 M KOH at a sweep rate of 5 mV s^{-1}; (c) The CV curves of NC in O_2-saturated (solid line) or N_2-saturated (dash line) in 0.1 M KOH at a sweep rate of 10 mV s^{-1}; (d) The LSV curve of NC in O_2-saturated 0.1 M KOH at a sweep rate of 5 mV s^{-1}.

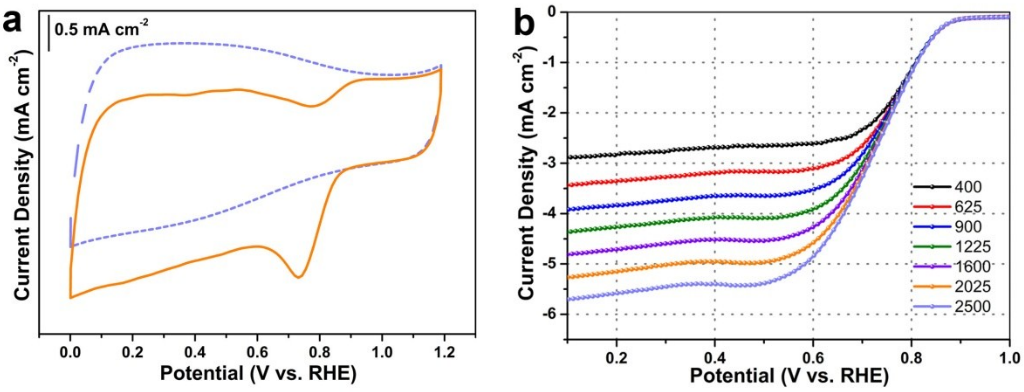

Fig. S23 (a) The CV curves of Fe subclusters decorated catalyst with 15 mg ferric nitrate in the synthesized process in O_2-saturated (solid line) or N_2-saturated (dash line) in 0.1 M KOH at a sweep rate of 10 mV s^{-1}; (b) The corresponding LSV curves in O_2-saturated 0.1 M KOH at a sweep rate of 5 mV s^{-1}.

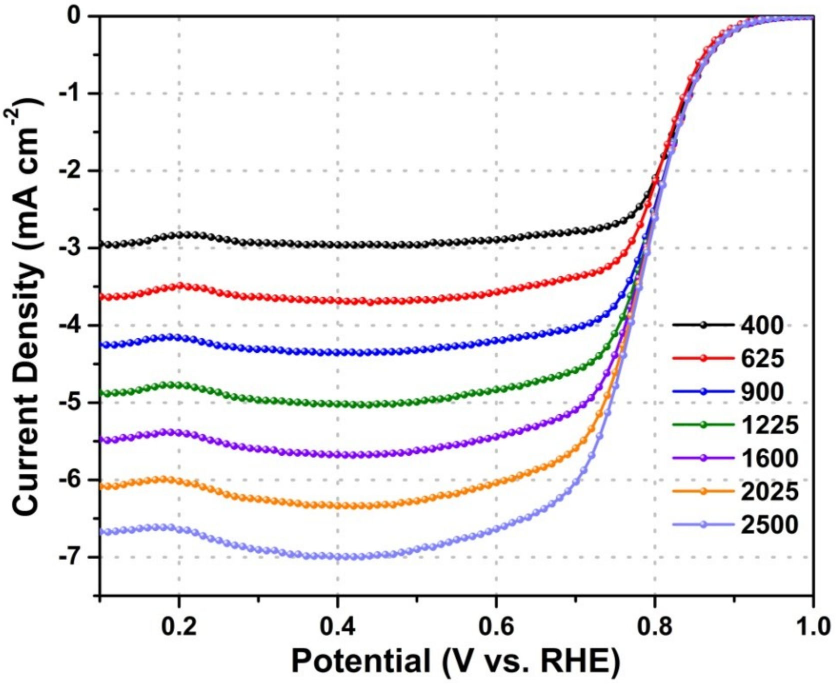

Fig. S24 The LSV curves of Pt/C in O_2-saturated 0.1 M KOH at a sweep rate of 5 mV s^{-1}.

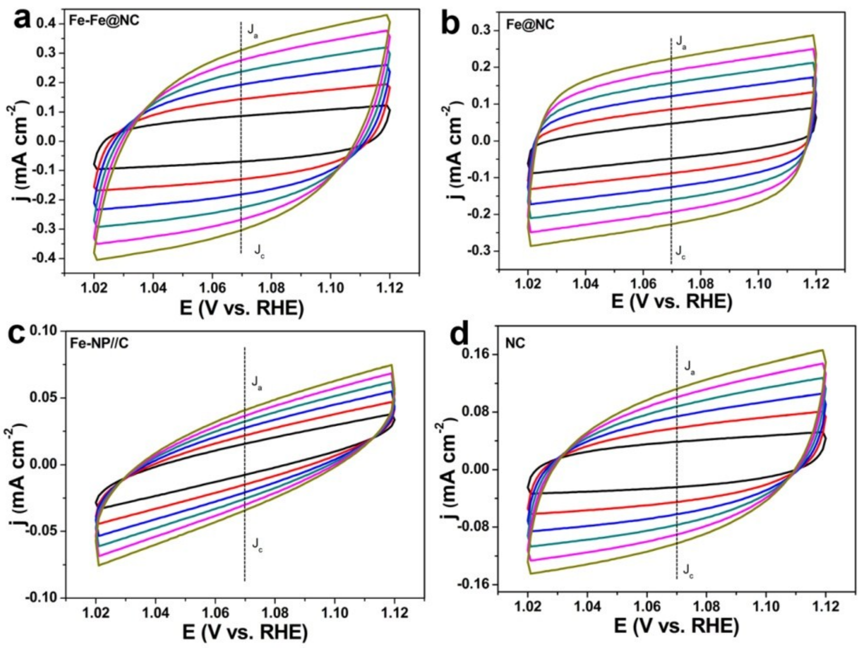

Fig. S25 Electrochemical capacitance measurements for the estimation of the electrochemical active surface area of catalysis; cyclic voltammograms of the (a) Fe-Fe@NC, (b) Fe@NC, (c) Fe-NP/C, (d) NC modified electrode at various scan rates.

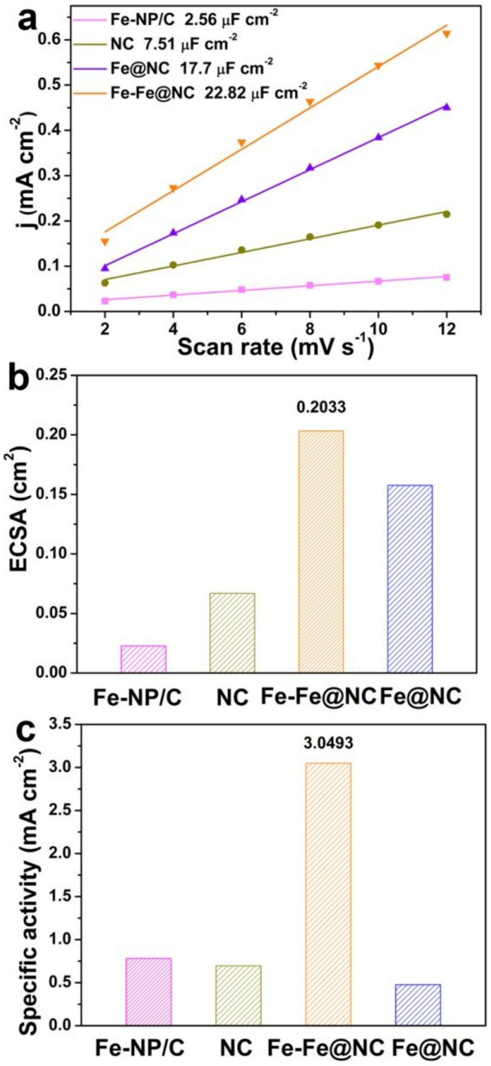

Fig. S26 (a) CDl. (b) the electrochemically active surface area (ECSA). (c) specific activity of samples.

In order to compare the activity for different catalysts, the kinetic currents were normalized with respect to the ECSA. As shown in Fig. S25, the Fe-Fe@NC exhibits a specific activity of 3.04 mA cm^{-2} at 0.8 V, which is much higher than reference catalysts.

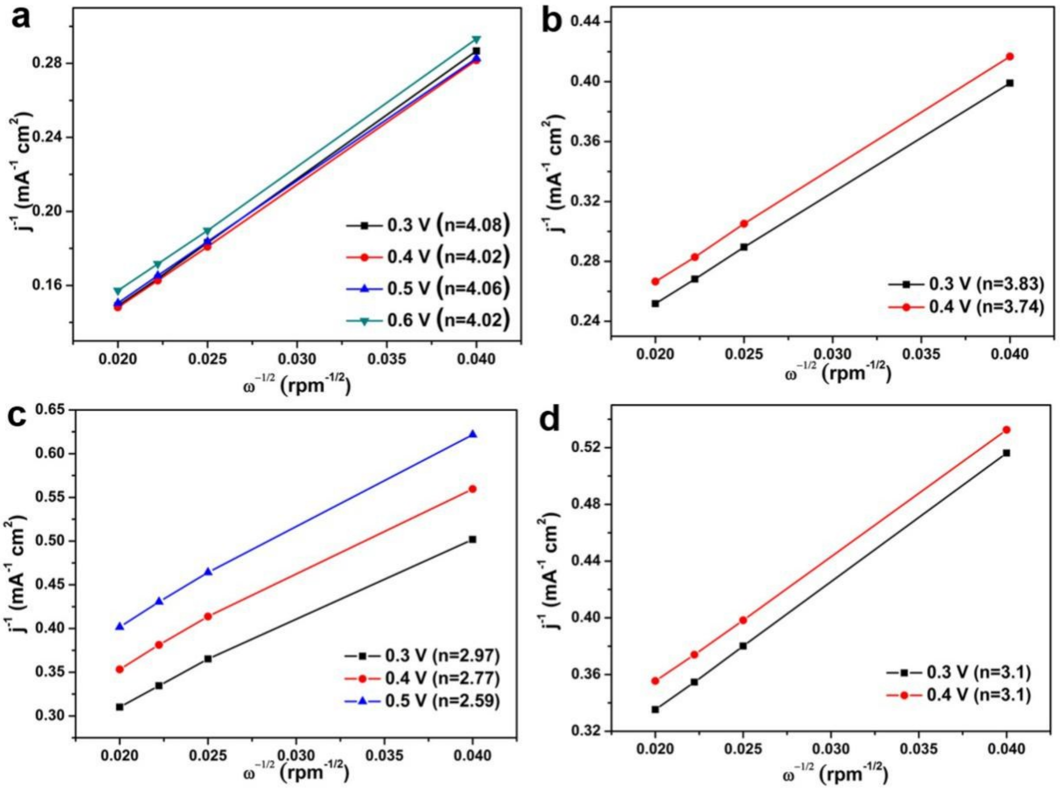

Fig. S27 Koutecky-Levich plots (J^{-1} vs $\omega^{-1/2}$) at different potentials of Pt/C (a), Fe@NC (b), Fe-NP/C (c) and NC (d).

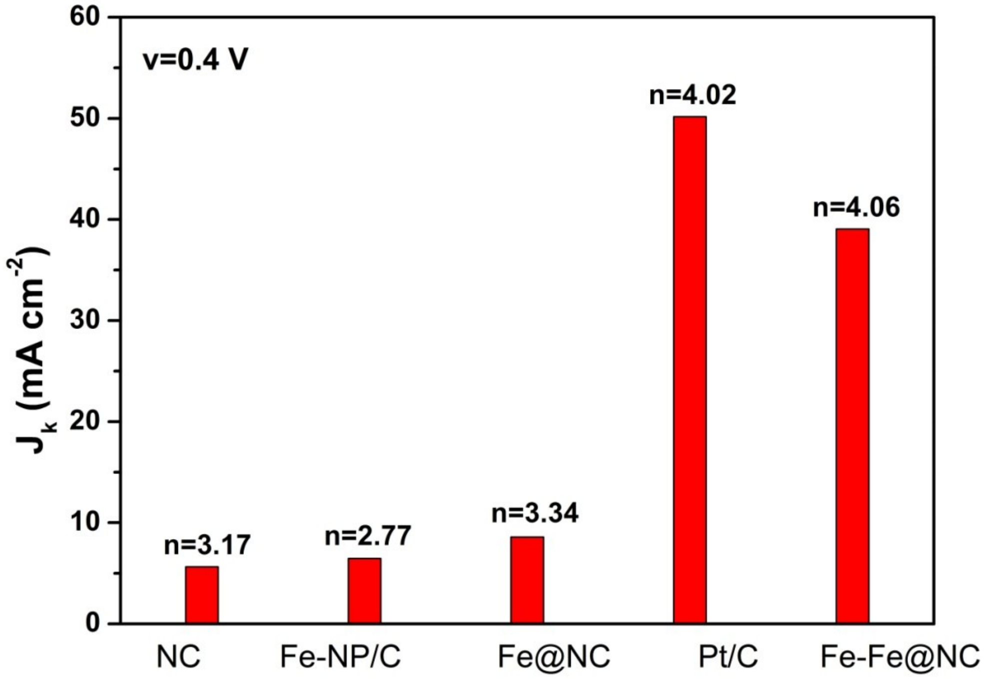

Fig. S28 The kinetic currents (J_k) of all samples.

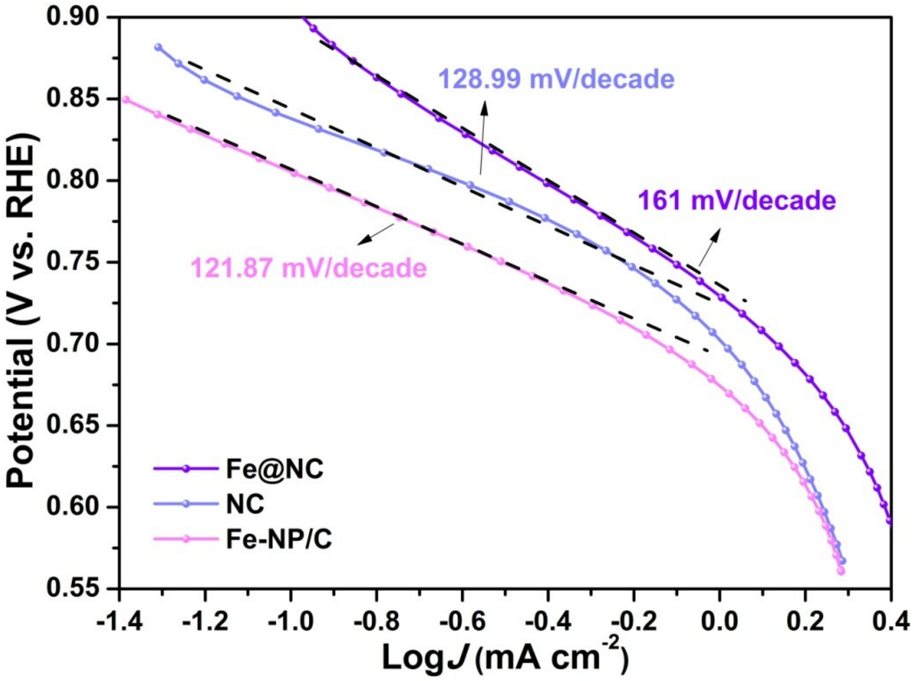

Fig. S29 Tafel plots of Fe@NC, Fe-NP/C and NC.

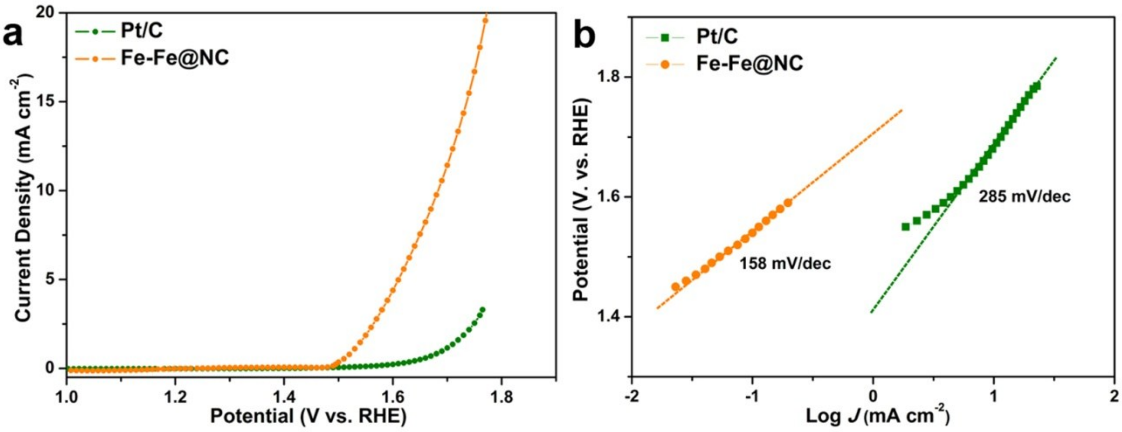

Fig. S30 (a) OER polarization curves of Fe-Fe@NC and Pt/C. (b) The corresponding Tafel plots.

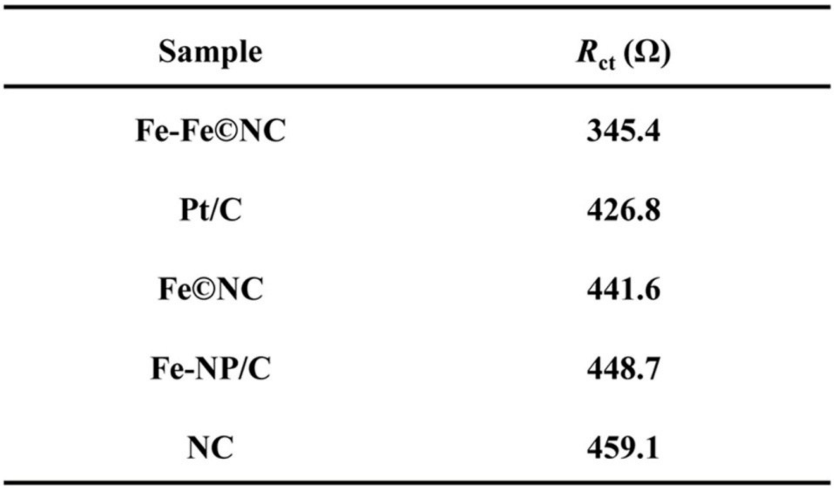

Sample	R_{ct} (Ω)
Fe-Fe©NC	345.4
Pt/C	426.8
Fe©NC	441.6
Fe-NP/C	448.7
NC	459.1

Fig. S31 The R_{ct} values of samples.

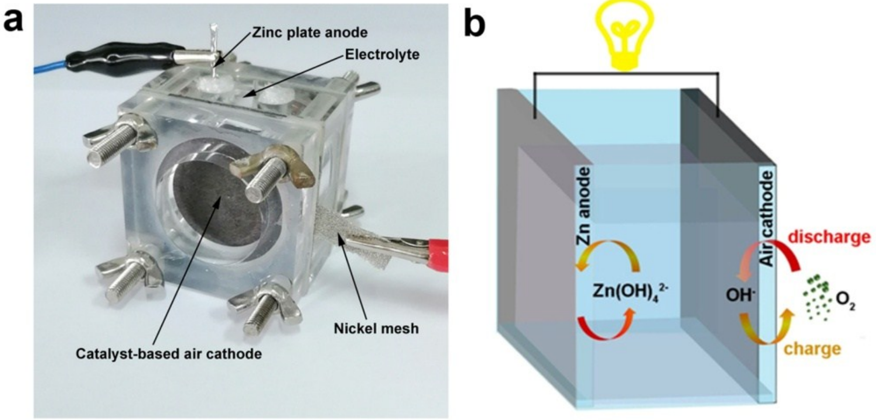

Fig. S32 (a) The fabrication of Zn-air battery assembly. (b) Schematic depiction of the rechargeable Zn–air battery. All the Zn-air batteries were tested at 25 ^{o}C under ambient atmosphere. The diacharge polarization curve measurements were measured by LSV (5 mV·s^{-1}) with electrochemical working station (Pine). The polarization and corresponding power density profiles were normalized to the effective surface area of air electrode. The specific capacity (mAh·g^{-1}) was calculated according to the equation below:

$$\frac{current * service\ hours}{weight\ of\ consumed\ zinc}$$

Galvanostatic discharge curves and mechanically recharged Zn-air battery were performed by LAND (100 mA) testing system.

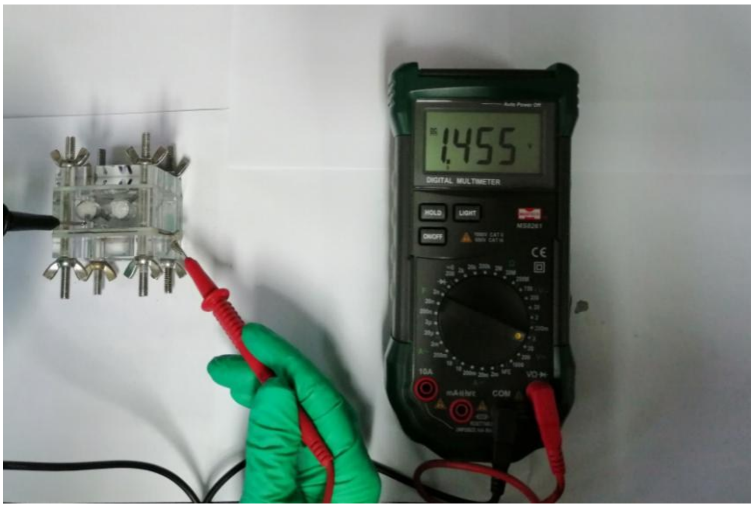

Fig. S33 Photograph of Zn-air battery using Fe-Fe@NC as cathode with an open circuit voltage of 1.45 V.

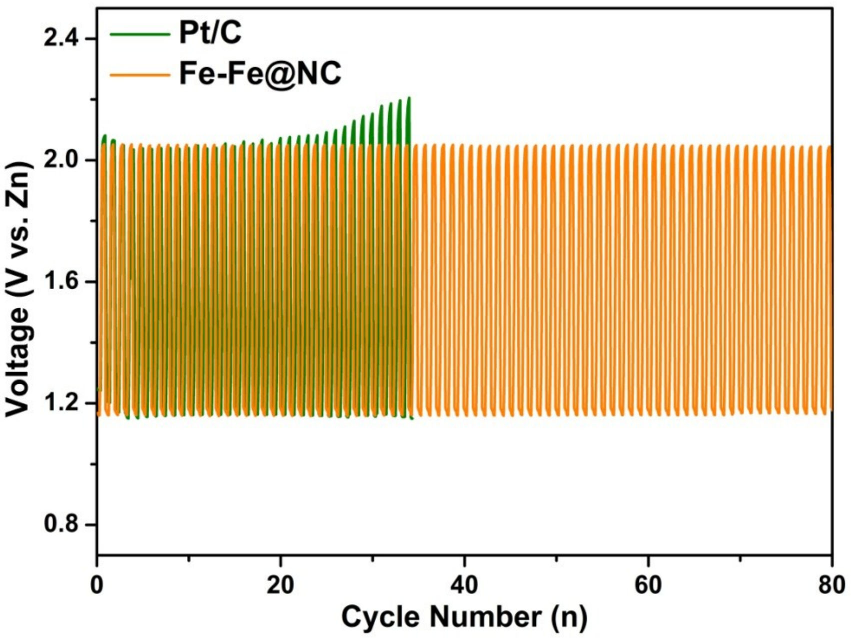

Fig. S34 Galvanostatic charge–discharge cycling performance of rechargeable Zn-air battery based on Fe-Fe@NC and Pt/C electrocatalysts at a constant charge-discharge current density of 10 mA cm^{-2}.

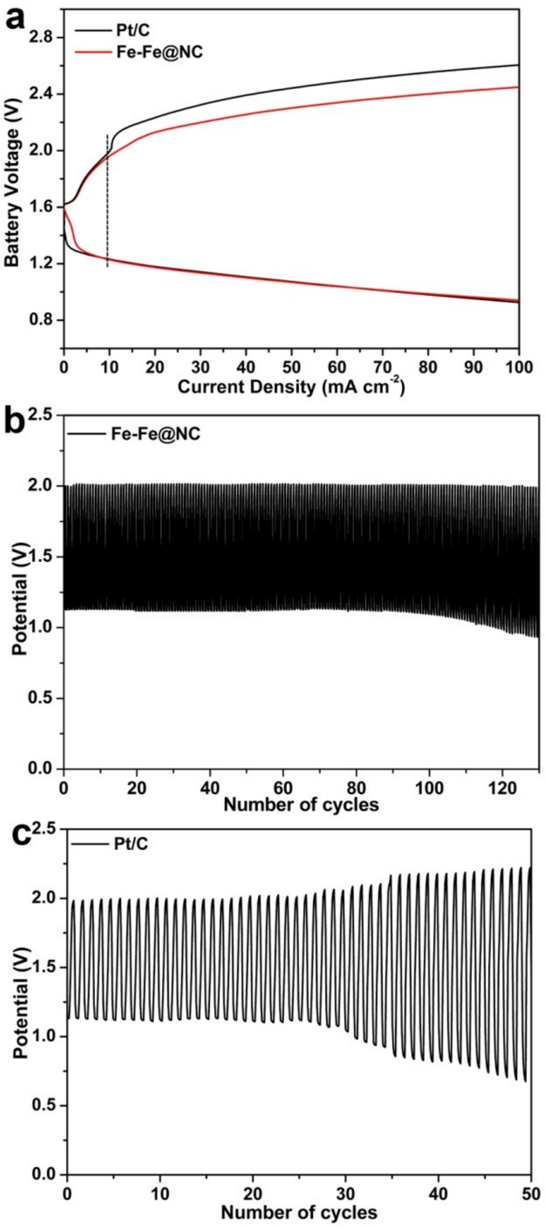

Fig. S35 (a) Charge and discharge polarization curves of Fe-Fe@NC and Pt/C samples. Galvanostatic charge–discharge cycling performance of rechargeable Zn-air battery based on Fe-Fe@NC (b) and Pt/C (c) electrocatalysts at a constant charge-discharge current density of 10 mA cm^{-2}.

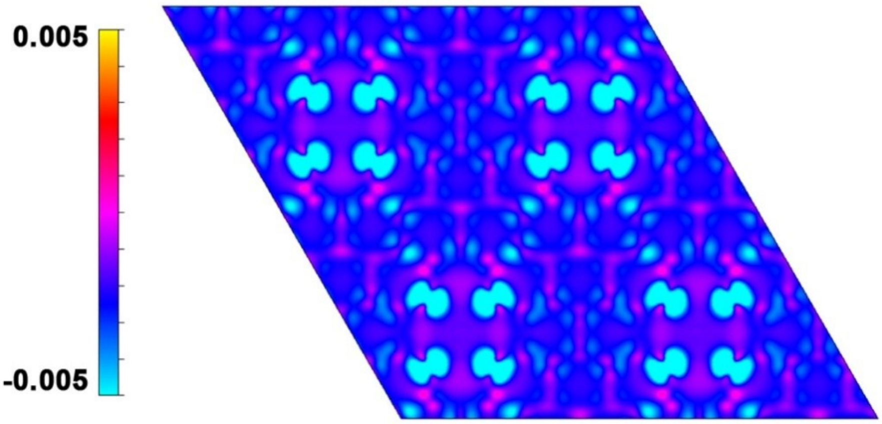

Fig. S36 The distribution of charge densities of NC.

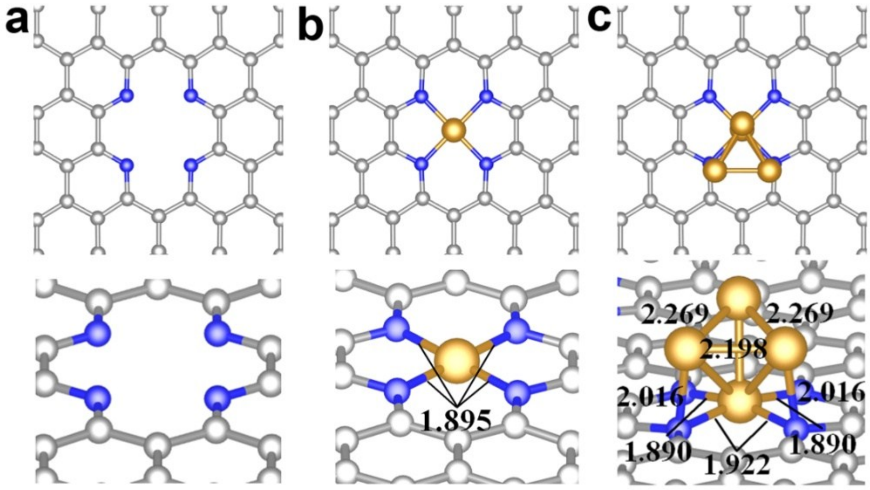

Fig. S37 The top and side views of the most stable configuration and partial geometry parameters (Å) for NC (a), Fe@NC (b) and Fe-Fe@NC (c) systems. C: gray N: blue Fe: brown.

Table S1. Fe K-edge EXAFS curve Fitting Parameters[a]

sample	shell	N	EXAFS (Å)	σ^2 (Å^2)	ΔE_0 (eV)	R, %
Fe@NC[b]	Fe−N	6.2	2.01	0.012	4.0	0.05
	Fe−C	3.4	3.23	0.008		
Fe-Fe@NC[c]	Fe−N	4.6	1.98	0.009	3.0	0.3
	Fe−C	3.1	2.76	0.012	3.0	
	Fe−C	5.8	3.47	0.004	3.0	
	Fe−Fe	2.5	2.55	0.009	5.8	
Fe-NP/C[b]	Fe−N	2.9	1.99	0.009	2.7	0.6
	Fe−C	2.6	2.80	0.010	0.1	
	Fe−Fe	4.2	2.48	0.010	0.1	

[a] N, coordination number; R, distance between absorber and backscatter atoms; σ^2, Debye–Waller factor to account for both thermal and structural disorders; ΔE_0, inner potential correction; R factor (%) indicates the goodness of the fit. Error bounds (accuracies) that characterize the structural parameters obtained by EXAFS spectroscopy were estimated as $N \pm 20\%$; $R \pm 1\%$; $\sigma^2 \pm 20\%$; $\Delta E_0 \pm 20\%$. S_0^2 was fixed to 0.93 as determined from Fe foil fitting. [b] Fitting range: $2.0 \leq k$ (/Å) ≤ 11.0 and $1.0 \leq R$ (Å) ≤ 2.8. [c] Fitting range: $2.0 \leq k$ (/Å) ≤ 11.0 and $1.1 \leq R$ (Å) ≤ 3.2.

Table S2. Surface areas and pore parameters of the prepared samples.

Materials	BET surface (m^2 g^{-1})	Pore volume (cm^3 g^{-1})	Average pore diameter (nm)
Fe-Fe@NC	433.55	0.35	3.26
Fe@NC	421.3	0.32	3.12
NC	387.09	0.26	2.97
Fe-NP/C	18.82	0.04	9.3

Table S3. Summary of representative ORR catalysts in varied electrolyte.

Materials	Surface area ($m^2 \cdot g^{-1}$)	Electrolyte	Loading mg/cm^2	ORR onset potential	ORR half-wave potential	Ref.
Fe-Fe@NC	433	0.1 M KOH	0.15	0.95 V vs. RHE	0.82 V vs. RHE	**This work**
Fe(0)@FeNC	240	0.1 M KOH	0.3	0.946 V vs. RHE	0.852 V vs. RHE	*Appl. Catal. B Environ.* **2019**, *251*, 240.
Fe-N-DSC	680	0.1 M KOH	0.102	0.061 vs. Ag/AgCl	-0.131V vs. Ag/AgCl	*ACS Nano*, **2018**, *12*, 208-216.
p-Fe-N-CNFs	941.015	0.5 M H_2SO_4	0.6	0.85 V vs. RHE	0.74V vs. RHE	*Energy Environ. Sci.* **2018,** *11,* 2208.
ZnN_x/BP	1383.9	0.1 M KOH	0.39	0 V vs. Ag/AgCl	0.175 V vs. Ag/AgCl	*Adv. Funct. Mater.* **2017**, *27*, 1700802
20Co-NC-1100	565	0.5 M H_2SO_4	0.8	0.93V vs. RHE	0.8 V vs. RHE	*Adv.Mater.* **2018,** *30,* 1706758.
Co-SAs@NC	130.7	0.1 M KOH	0.612	0.96V vs. RHE	0.82V vs. RHE	*Angew. Chem. Int. Ed.* ***2019***, *58,* 5359-5364.
FeN_x/GM	1070	0.5 M H_2SO_4	0.6	--	0.80 V vs. RHE	*Adv. Energy Mater.* **2019**, *9,* 1803737.
FeSA-G	--	0.1 M $HClO_4$	0.3	0.95 V vs. RHE	0.804 V vs. RHE	*Adv. Sci.* ***2019***,*6,* 1802066.
SA-Fe-HPC	1436.3	0.1 M H_2SO_4	0.1	--	0.81 V vs. RHE	*Angew. Chem. Int. Ed.* ***2018***, *57,* 1-7.
H-Fe-N_x-C	917	0.5 M H_2SO_4	0.19	--	0.77 V vs. RHE	*ACS Nano* **2019**, *3,* 8087-8098.
FNCT800-100	368.33	0.1 M KOH	0.2	-0.038 vs. Ag/AgCl	-0.143 vs. Ag/AgCl	*Nanoscale,* **2017**, *9,* 17364-17370.
Co,N-PCL	319	0.1 M KOH	0.2	--	0.846 V vs. RHE	*Appl. Catal. B Environ.* **2019**, *246*, 322.
Ru-N/G-750	395.49	0.1 M $HClO_4$	0.35	0.89 V vs. RHE	0.75 V vs. RHE	*ACS Nano*, **2017**, *11,* 6930-6941.
Co-N/C	283.2	0.1 M KOH	0.254	0.916 V vs. RHE	0.825 V vs. RHE	*Nanoscale Horiz.*, **2019**, *4*, 1006.

Table S4. Summarized properties of our and recently reported Zn-air batteries

Materials	Loading amount (mg/cm^2)	open-circuit voltage (V)	The maximum power density (mW cm^{-2})	Ref
Fe-Fe@NC	2	1.45	175	This work
NSC-1000	2	1.4	167.8	*Nano Energy* **2019**, DOI:10.1016/j.nanoen.2019.02.043.
CMO/S-300	1	1.4	152	*Adv. Energy Mater.* **2018**, *8*, 1800612.
Mo-N/C@MoS$_2$	5	1.46	196.4	*Adv. Funct. Mater.* **2017**, *27*, 1702300.
β-FeOOH/PNGN s	--	1.45	160	*Adv. Funct. Mater.* **2018***, 28,* 1803330.
(Zn,Co)/NSC	1	1.5	150	*Nano energy,*
Co-N$_x$-B$_y$-C	--	1. 4	100.4	*ACS Nnao* **2018***,* **12***,* 1894-1901.